Supplementary Information for "Grain boundary-mediated nanopores in molybdenum disulfide grown by chemical vapor deposition"

Atomic force microscopy and Raman spectroscopy analysis

A Raman spectrum indicating the in-plane E^1_{2g} and out-of-plane A_{1g} modes of MoS_2 is shown in Supplementary Figure 1a. The peak positions of the E^1_{2g} and A_{1g} Raman modes are ca. 382 cm^{-1} and ca. 405 cm^{-1}, which confirm[40,41] the formation of BL MoS_2 (Ref. [42]). The 2LA(M) Raman peak is also observed at the position of ca. 452 cm^{-1} (Refs. [43,44]). Supplementary Figure 1b shows a tapping mode AFM topography image of MoS_2 islands on top of a SiN/Si chip with multiple holes confirming that MoS_2 grains have triangular shapes.

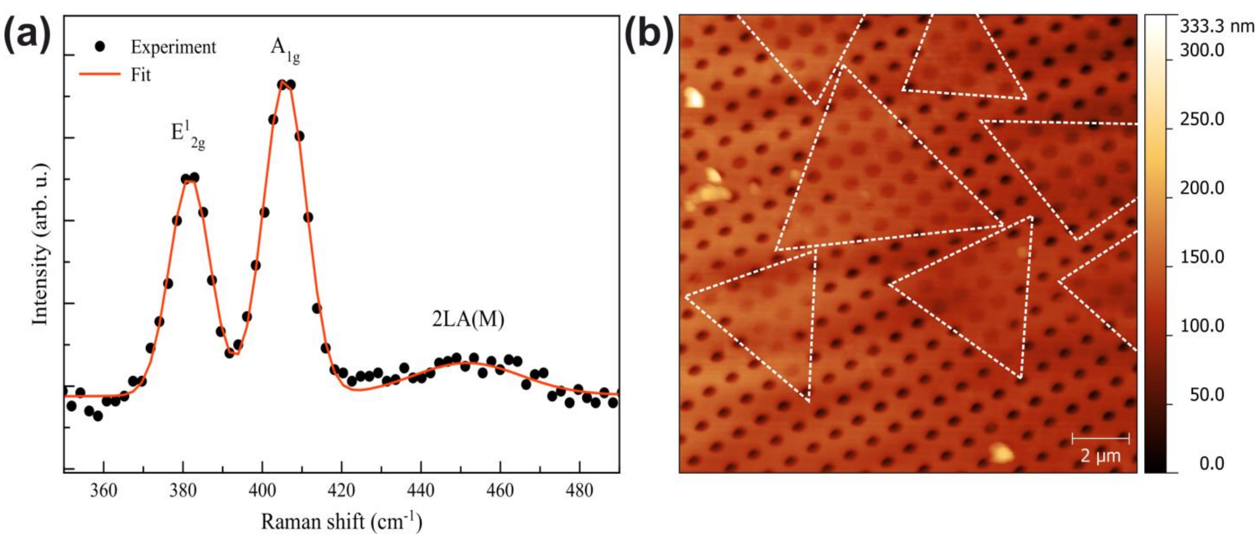

Supplementary Figure 1. (a) Raman spectrum of suspended MoS_2 showing in-plane E^1_{2g} and out-off plane A_{1g} Raman modes and the 2LA(M) peak measured with a 473 nm laser. (b) AFM topography image of four well-separated MoS_2 grains (highlighted with white lines) on a SiN/Si chip with multiple holes.

Pores between MoS_2 grains

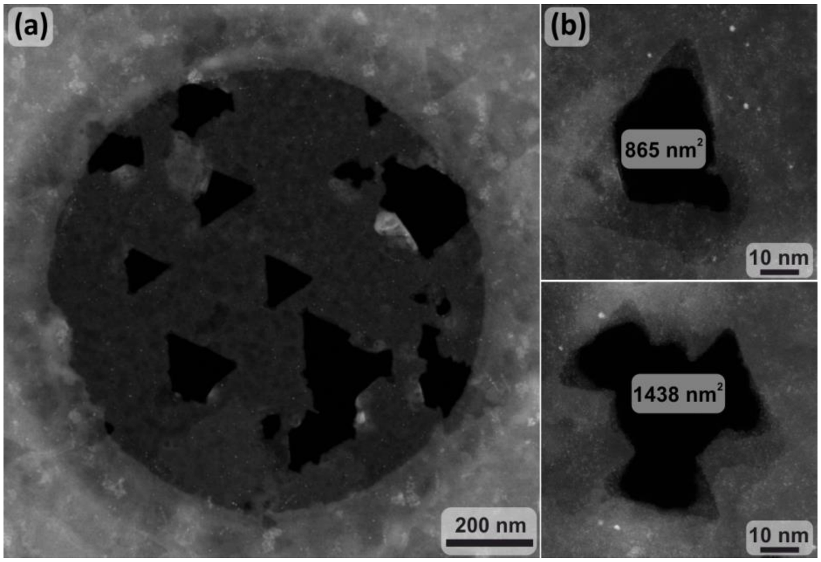

Supplementary Figure 2. HAADF-STEM images showing triangular holes between MoS_2 grains after prematurely terminated CVD growth.

Atomic structure of the dislocation core

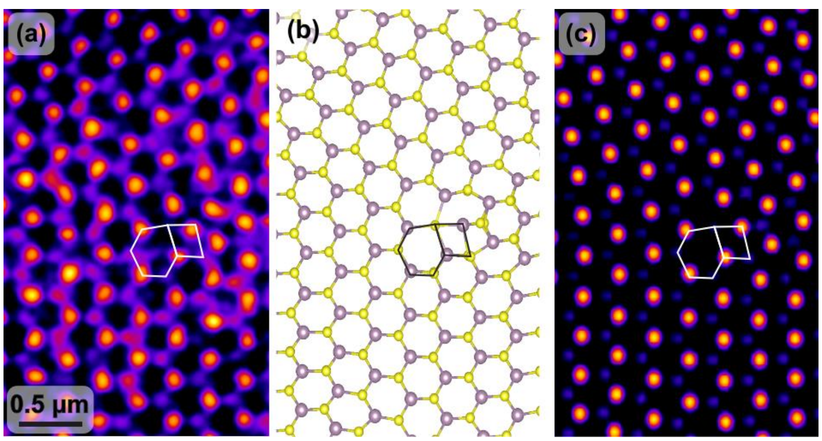

Supplementary Figure 3. (a) HAADF-STEM image showing the GB of ML MoS_2. (b) An atomistic model of the GB, relaxed by DFT, with a 4|6 dislocation. (c) Simulated HAADF-STEM image of the relaxed model in (b).

Edge dislocation models

The strain of an edge dislocation can be described by the Peierls–Nabarro (PN) and the Foreman (FM) models. These models are fitted to our experimental strain distribution around a dislocation core obtained by GPA. The strain of an edge dislocation along the *x* direction is given by PN and FM models as

$$\varepsilon_{xx}^{PN} = -\frac{b}{\pi}\left[\frac{(1-v)y}{4(1-v)^2x^2+y^2}\right] \tag{1}$$

and

$$\varepsilon_{xx}^{FM} = -\frac{b(1-v)}{\pi}\left[\frac{4(1-v)^2yx^2+(2a^3-a^2)y^3}{(4(1-v)^2x^2+a^2y^2)^2}\right]. \tag{2}$$

Here b is the magnitude of Burger vector, v the Poisson's ratio (0.25 for ML MoS_2)[46], and a a fitting parameter. In case of a = 1, FM model is equal to PN model.

Unfiltered version of Figure 5a

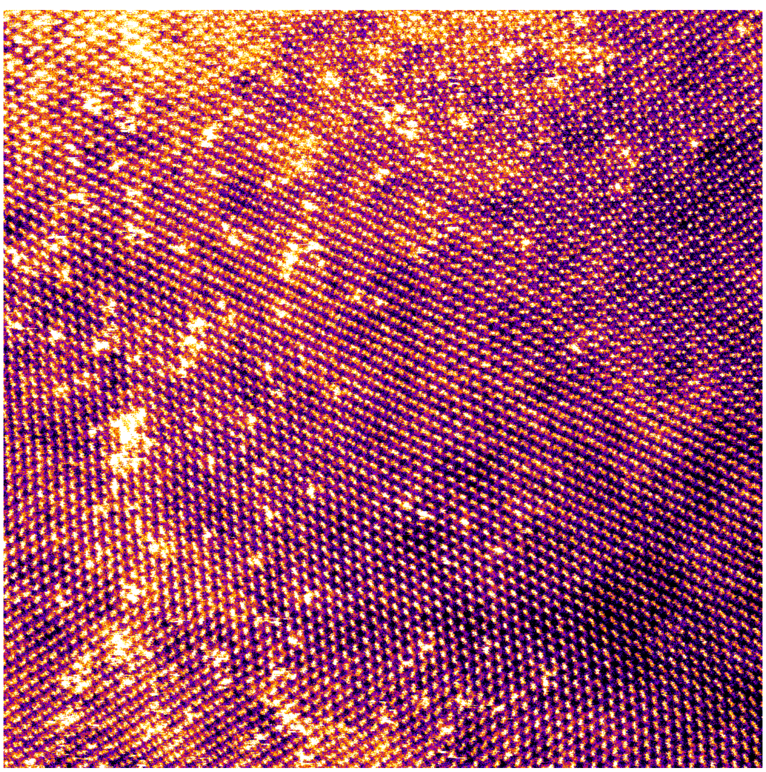

Supplementary Figure 4. Unprocessed HAADF-STEM image of bilayer MoS_2.

Analysis of the sample thickness and rippling of bilayers

In order to confirm the thicknesses of the studied films, we made image simulations for ML and BL MoS_2 and compared the intensity profiles of simulated and experimental images, as shown in Supplementary Figure 5. The thickness of layers can also be measured by diffraction experiments (Supplementary Figure 6) because the intensity ratio within the $\{\bar{1}100\}$ family in diffraction patterns of ML and BL MoS_2 gives information on layer thicknesses[45]. The intensity ratios in the $\{\bar{1}100\}$ family of ML MoS_2 show no tilt or ripple in ML MoS_2. In contrast, the intensity ratios for BL MoS_2 are in many cases not ~1 like they should be for a flat BL structure [45]. This indicates rippling in one or both of the layers since it can cause such intensity variations[45].

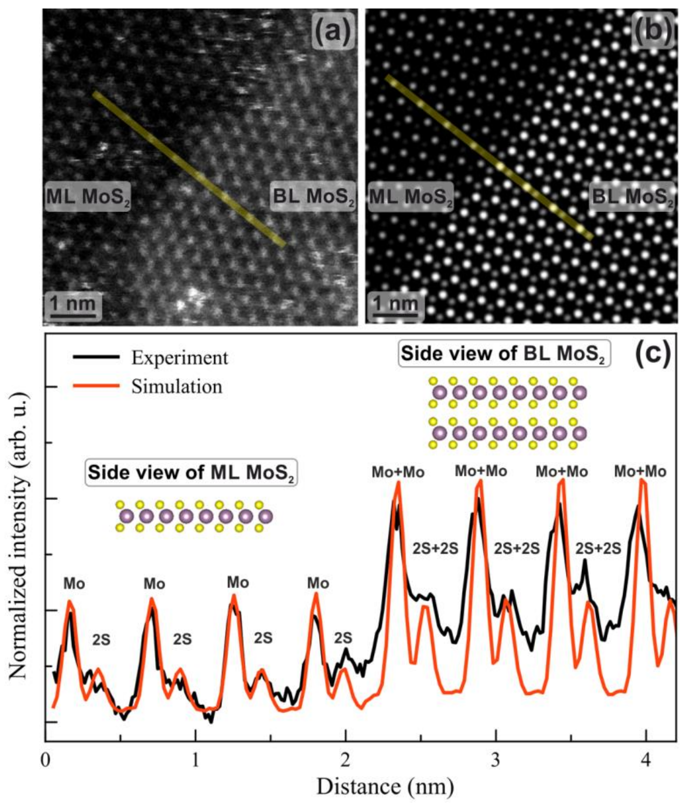

Supplementary Figure 5. (a) HAADF-STEM image showing ML and BL MoS_2. (b) The corresponding simulated HAADF image. (c) Intensity profiles along the yellow lines on experimental and simulated images.

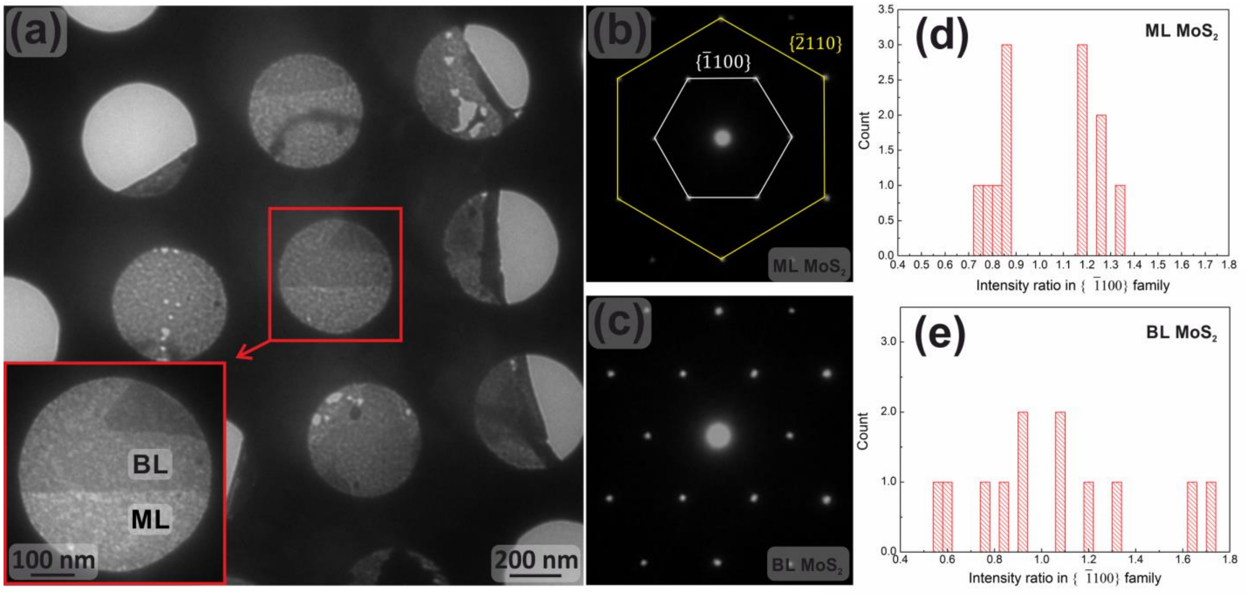

Supplementary Figure 6. (a) TEM image of CVD-grown MoS_2 on a holey SiN/Si chip. Inset is a close-up image showing ML and BL MoS_2 in the red square. (b) and (c) are the diffraction patterns for ML and BL MoS_2. (d,e) Histograms indicating the intensity ratio in the $\{\bar{1}100\}$ family for ML and BL MoS_2 for several studied sample locations.

Electron beam-induced nanopores

The MoS_2 GB-NPs shown in the main article have not been created by electron irradiation during the experiment. The formation of NPs under the beam is easily observed during the experiment and is not limited to GBs, as shown in Supplementary Figure 7. Interestingly shear strain maps of beam-induced NPs show that the amount of tensile strain on the sample is reduced during the NP formation while the regions with compressive strain grow. In contrast, the GB-NPs are more tensile strained owing to dislocation cores inducing high levels of strain.

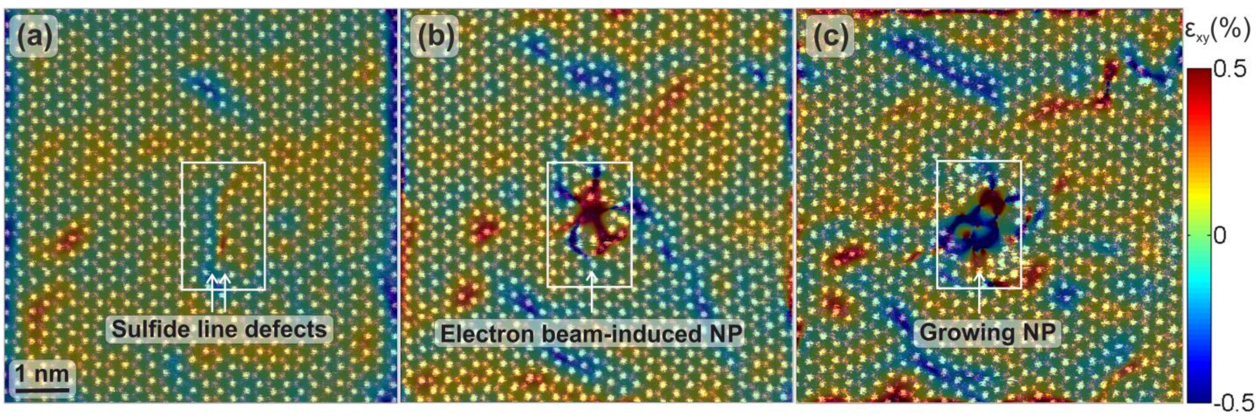

Supplementary Figure 7. HAADF-STEM images of MoS_2 with a nanopore induced by the electron beam, superimposed with their shear strain maps. (a) Sulfide line defects created during STEM imaging at 60 kV. (b) Formation of the MoS_2 NP approximately 30 seconds later. (c) Growing MoS_2 NP approximately 50 seconds later. Red and blue correspond to tensile and compressive strain, respectively.

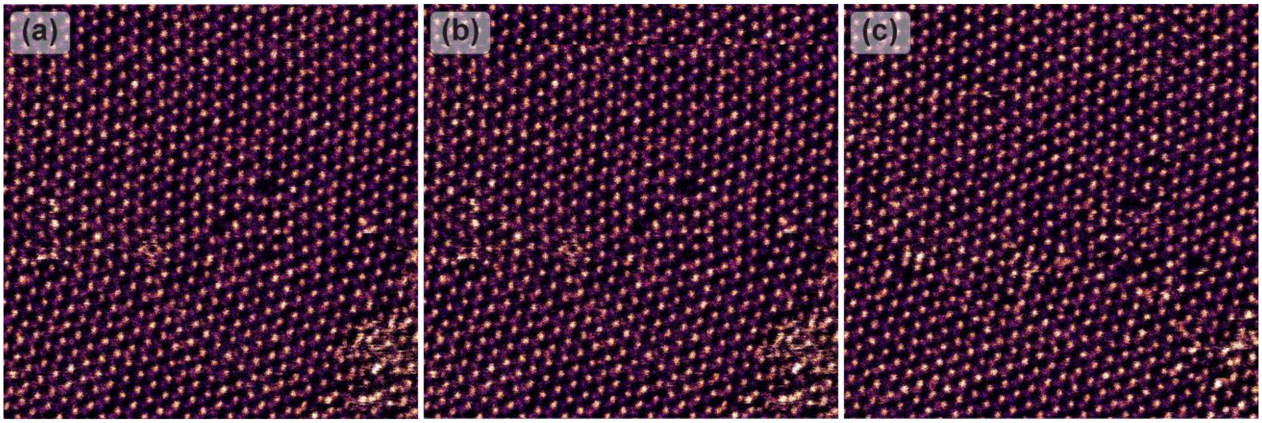

Supplementary Figure 8. HAADF-STEM images of MoS_2 grain boundary. (a) First scan. (b) 5 seconds later. (c) 50 seconds later.

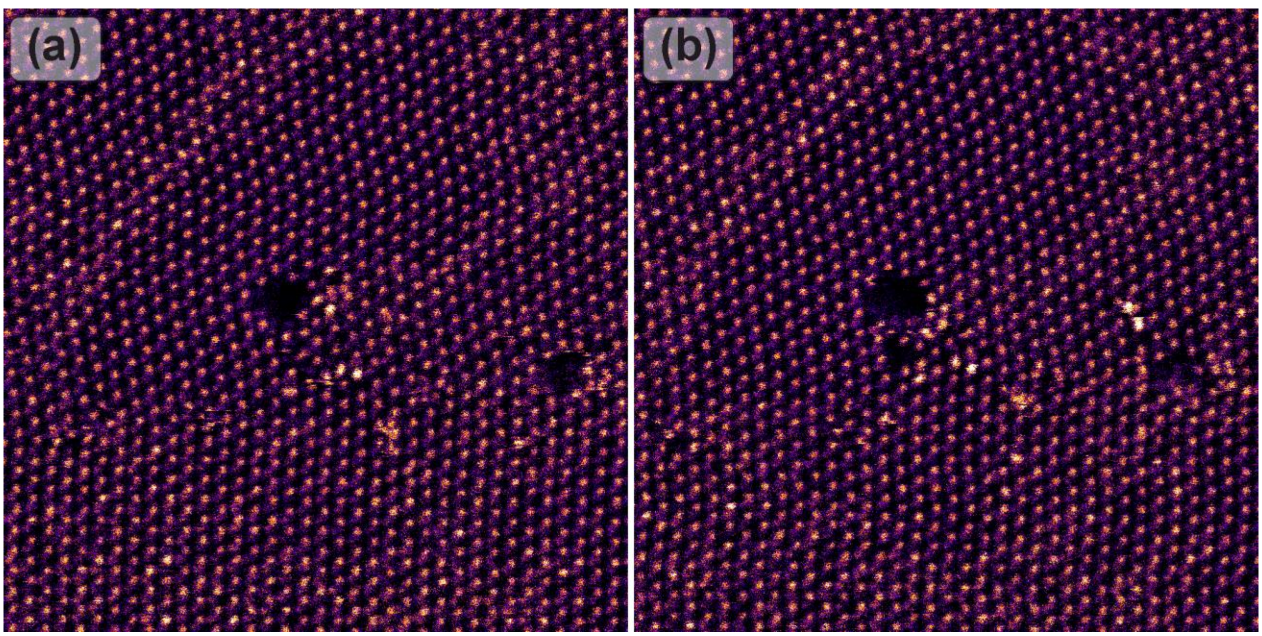

Supplementary Figure 9. HAADF-STEM images of MoS_2 grain boundary. (a) first scan. (b) 40 seconds later.

Theoretical results on the bilayer structure in overlap areas

Supplementary Table 1. DFT results for different stacking orders of BL MoS_2.

Stacking	Total energy (eV)	Interlayer distance (Å)	Band gap (eV)
AA	22.971	6.94	1.24
AB	22.926	6.52	0.99
AB-AA	22.969	7.08	1.26

References

References are listed in the main article.